A non-spiking neuron model with dynamic leak to avoid instability in recurrent networks

Udaya B. Rongala[1*], Jonas M.D. Enander[1], Matthias Kohler[2], Gerald E. Loeb[3], Henrik Jörntell[1]

[1] Department of Experimental Medical Science, Faculty of Medicine, Lund University, Lund, Sweden

[2] Department of Informatics, Technical University of Munich, 85748 Garching, Germany

[3] Department of Biomedical Engineering, Viterbi School of Engineering, University of Southern California, Los Angeles, CA, USA

*Corresponding author

E-mail: udaya_bhaskar.rongala@med.lu.se (UBR)

Abstract

Recurrent circuitry components are distributed widely within the brain, including both excitatory and inhibitory synaptic connections. Recurrent neuronal networks have potential stability problems, perhaps a predisposition to epilepsy. More generally, instability risks making internal representations of information unreliable. To assess the inherent stability properties of such recurrent networks, we tested a linear summation, non-spiking neuron model with and without a 'dynamic leak', corresponding to the low-pass filtering of synaptic input current by the RC circuit of the biological membrane. We first show that the output of this neuron model, in either of its two forms, follows its input at a higher fidelity than a wide range of spiking neuron models across a range of input frequencies. Then we constructed fully connected recurrent networks with equal numbers of excitatory and inhibitory neurons and randomly distributed weights across all synapses. When the networks were driven by pseudorandom sensory inputs with varying frequency, the recurrent network activity tended to induce high frequency self-amplifying components, sometimes evident as distinct transients, which were not present in the input data. The addition of a dynamic leak based on known membrane properties consistently removed such spurious high frequency noise across all networks. Furthermore, we found that the neuron model with dynamic leak imparts a network stability that seamlessly scales with the size of the network, conduction delays, the input density of the sensory signal and a wide range of synaptic weight distributions. Our findings suggest that neuronal dynamic leak serves the beneficial function of protecting recurrent neuronal circuitry from the self-induction of spurious high frequency signals, thereby permitting the brain to utilize this architectural circuitry component regardless of network size or recurrency.

Author Summary

It is known that neurons of the brain are extensively interconnected, which can result in many recurrent loops within its neuronal network. Such loops are prone to instability. Here we wanted to explore the potential noise and instability that could result in recurrently connected neuronal networks across a range of conditions. To facilitate such simulations, we developed a non-spiking neuron model that captures the main characteristics of conductance-based neuron models of Hodgkin-Huxley type, but is more computationally efficient. We found that a so-called dynamic leak, which is a natural consequence of the way the membrane of the neuron is constructed and how the neuron integrates synaptic inputs, provided protection against spurious, high frequency noise that tended to arise in our recurrent networks of varying size. We propose that this linear summation model provides a stable and useful tool for exploring the computational behavior of recurrent neural networks.

Introduction

Recurrent excitatory loops are a common feature in the central nervous system, such as in neocortical circuits [1–4], thalamocortical loops [5,6], cerebrocerebellar and spinocerebellar loops [7,8]. Inhibitory interneurons have been described to provide lateral inhibition [9–12] and feed-forward inhibition [13,14], but they also make synapses on other inhibitory neurons, thereby potentially forming recurrent disinhibitory loops as well [15–17]. Furthermore, such excitatory and inhibitory connectivity has been reported to be balanced [18–20]. Functionally, recurrent connections enable a network to use preceding states to impact the processing of the present state. Such state memory can, for example, improve learning performance [21]. However, due to the many potential positive feedback loops in larger networks with extensive recurrent connections, imbalances in excitatory (E) and inhibitory (I) synaptic activity could lead to activity saturation [22,23], such as observed in epilepsy [24,25], or, in milder cases, a noise-like perturbation of the information content of internal signals, which would be disadvantageous for learning.

We explored potential noise and stability issues that could arise in recurrent neuronal networks. In order to focus on the network architecture aspect of this problem, we used a non-spiking neuron model designed to be simple and computationally efficient, while embodying fundamental properties of Hodgkin-Huxley conductance-based models. The relevance of a non-spiking neuron model stems from the stochasticity inherent in neuronal spike generation [26–28], which renders the spiking output of the individual neuron to some degree unreliable in terms of information content. To compensate for such unreliability, the brain could encode each representation across a population of neurons (below referred to as an ensemble of redundant neurons), as has been observed in the brain *in vivo* [29]. The input-output relationships across a range of neuron types in the central nervous system *in vivo* indicate that overall, each neuron's spike output is a probability density function (PDF) of the underlying

membrane potential of the neuron [27]. That PDF thereby approximates the membrane potential and could be considered to correspond to the spike output of an ensemble of neurons with similar inputs. Thus, simulating a non-spiking neuron and providing the PDF of the neuron as its output avoids the extreme resource demands of both simulating the highly complex spike generation stochasticity [28] and compensating for that stochasticity by simulating large populations of redundant neurons. Synaptic input creates modulation of the neuronal membrane potential, hence its PDF, by temporarily activating conductances that are added to the static leak conductances. The synaptic conductances and currents can modulate very rapidly but the membrane capacitance together with the static leak channels forms an RC circuit that constitutes a low-pass filter (herein, dynamic leak) for the resultant membrane potential. We hypothesized that this dynamic leak would improve network stability without compromising information transfer.

To test this hypothesis, we constructed a highly recurrent, two-layer neuronal network, with five excitatory and five inhibitory neurons in the first layer and four excitatory and four inhibitory neurons in the second layer. All neurons in both layers were reciprocally connected with randomized gains. All first layer neurons were provided with six randomized and broadly distributed input signals. A striking finding was that for all tested network configurations, synaptic weight distributions, various conduction delays and input density of sensory inputs, recurrent networks tended to generate high frequency components that were not present in the sensory input data. In all cases these transients were eliminated by incorporating a dynamic leak in the neuron models without compromising the representation of the input signals.

We note that the fully reciprocal connectivity employed in the networks described herein encompasses the wide range of connectivity that has been identified experimentally in cortical and other central neural structures (see above). The strictly layered connectivity of many popular neural network models for deep learning reflects only a small subset of the

known complexity of biological networks. Attempts to add limited recurrency into such models have encountered stability problems [22,23], for which dynamic leak appears to offer substantial mitigation.

Methods

Neuron model

Linear summation neuron model (LSM): The neuron model implemented for this study was a non-spiking, linear input summation model with an additional dynamic leak component. For the version without dynamic leak, the activity ($A_{No_{Dyn}}$) was given by the total weighted input activity ($w * a$) (where a is the activity of each individual input and w is the weight of that input) across all individual synapses (i) (Eq. 1). Electrotonic compactness in the neuron is assumed, so that all synapses have equal impact on the activity of the neuron. This simplified model of synaptic input activity integration can be shown to be closely related to a Hodgkin-Huxley (H-H) model (see Appendix 1), for example resulting in the preservation of two key dependencies of EPSPs and IPSPs on membrane biophysics: *i*) input response magnitude depends on the difference between the membrane potential and the reversal potentials for the relevant corresponding 'ion channels' (i.e. depending on if the input is provided through an excitatory or an inhibitory synapse); *ii*) input response magnitude depends on relative shunting of synaptic currents by conductances resulting from the background of synaptic input activity (Eq. 1). The responsive properties of the LSM and the H-H neuron model are shown to be highly similar in S1 Fig.

The LSM implemented a degree of activity normalization (denominator of Eq. 1) by introducing a static leak, which was calculated as the product of a constant (k_{static}) multiplied by the number of synapses on the neuron, plus a term reflecting the total number of open channels, which is activity dependent.

To mimic the effect of the RC circuit created by the ion channels and the capacitance of the membrane, we added a dynamic leak function to the neuron. To test the impact of the dynamic leak on network dynamics, we compared the networks composed of neurons with the dynamic leak with the same network when the neuron model did not include this dynamic leak. The neuron activity for the neuron model variant with dynamic leak (A_{Dyn}) is given by the linear summation model with an additional leak time constant (τ_{Dyn}). Larger neurons with more synapses tend to have longer time constants [30], so we tried various ways of scaling τ_{Dyn} with number of synapses i. Thereby, the dynamic leak integrates the function of the capacitance in the RC circuit of the biological neuron into the LSM (Eq. 2). The neuron activity of this model is given by the following equations,

$$A_{No_{Dyn}} = \frac{\sum(w_i * a_i)}{(k_{static} * i) + \sum|w_i * a_i|} \tag{1}$$

$$\frac{\tau_{Dyn} * dA_{Dyn}}{dt} = -A_{Dyn}(t) + A_{No_{Dyn}}(t) \tag{2}$$

$$\begin{gathered} 0 \leq A_{No_{Dyn}} \\ 0 \leq A_{Dyn} \end{gathered} \tag{3}$$

Figure 1 illustrates the output activity of individual LSM neurons (Eq. 1-3), which were isolated in the sense that they were not connected to any neuronal network other than the provided inputs, for different input combinations of emulated excitatory and inhibitory synaptic inputs (Fig 1A, B). The input spike trains were convoluted using a kernel function in order to emulate post-synaptic-potential inputs (detailed below, Eq. 6), that were fed to the LSM neuron (Fig 1C-E). The LSM activity without dynamic leak ($A_{No_{Dyn}}$, Fig 1F) shows the activity normalization resulting from the static leak constant ($k_{static} = 1$, for this illustration), along with the effect of the neuron output activity threshold at zero (Eq. 3). The activity of the LSM neuron would also be expected to fall back towards this zero level of activity without any

153 external or internal input. This level hence corresponds to a threshold for spike initiation among
154 a population of similarly connected neurons that are typically represented by the one modeled
155 neuron. The output activity for the LSM neuron with dynamic leak (A_{Dyn}, Fig 1G) exhibits a
156 low pass filtering effect on the output activity, which is reflective of the effect of the RC
157 component integrated in the LSM neuron model with the dynamic leak.

158 Figure 2 illustrates the impact of various static and dynamic leaks. As indicated in Fig
159 2A, the static leak constant acts as a normalization factor for the total neuron activity, without
160 diminishing the underlying dynamics of that activity (S2 Fig). At very low values of the static
161 leak constant, the mean activity reached sufficiently high levels for the reversal potential to
162 start having a significant dampening effect on the activity dynamics (see uppermost trace in
163 Fig 2A), substantially reducing the coefficient of variation (CV in Fig 2B). Fig 2C, D illustrates
164 the additional impact of various values of the dynamic leak constant. Fig 2C and S3 Fig
165 demonstrate the filtering effect of the dynamic leak constant on the total neuron activity. A
166 high value of this dynamic leak constant substantially smoothens the activity dynamics, which
167 was reflected in the resulting low CV value (Fig 2D). The dynamic leak constant (τ_{Dyn}) was
168 set to 1/100 for the rest of this study, unless otherwise specified.

169 In Appendix 1, we show that the LSM neuron model can be derived from a simplified
170 H-H type conductance-based neuron model. In the H-H model, the leak is proportional to the
171 membrane voltage and the synaptic currents are scaled depending on the membrane voltage,
172 so that the voltage is limited to a fixed range. The differential equation describing this model
173 suffers from numerical instability, therefore we solve it with the implicit Euler method. The
174 model is simple enough so that an analytical solution can be obtained. Key H-H model features
175 that are captured by the LSM neuron: *i*) the response to a given input scales with the difference
176 between the current activity level (membrane potential V) and the reversal potentials of the
177 excitatory/inhibitory inputs (which have been normalized to +1 and -1, respectively); and *ii*)

178 the impact of a given input is scaled by the degree of the shunting caused by the total synaptic
179 activity the neuron receives at that time.

180 **Izhikevich neuron model (IZ):** For the Izhikevich neuron model [31], the membrane potential
181 (IZ_v) and the adaptation variable (IZ_u) were updated via the following nonlinear differential
182 equations discretized using Euler's method.

$$\dot{IZ}_v = IZ_A IZ_v^2 + IZ_B IZ_v + IZ_C - IZ_u + (IZ_{input} * IZ_k)$$
$$\dot{IZ}_u = IZ_a(IZ_b IZ_v - IZ_u) \quad (4)$$

183 When the membrane potential reached the spike depolarization threshold of 30 mV, one spike
184 was produced followed by a reset:

$$if\ IZ_v \geq 30mV, then \begin{cases} IZ_v \leftarrow IZ_c \\ IZ_u \leftarrow IZ_u + IZ_d \end{cases} \quad (5)$$

185 The IZ_A, IZ_B & IZ_C parameters and the spiking threshold were the standard ones of the
186 Izhikevich artificial neuron model, whereas the parameters IZ_a, IZ_b, IZ_c & IZ_d were selected
187 (Table 1, Fig 3E, F) to mimic a regular spiking behavior [31,32]. IZ_{input} was the input current
188 to the neuron model, that was weighted synaptic activity ($w * a$) in this article and IZ_k is the
189 input gain factor.

190 **Table 1.** Izhikevich neuron model parameters used in the evaluation of this study. For the IZ
191 model responses presented in Fig 3E-F and S3 Fig.

IZ_A	IZ_B	IZ_C	IZ_a	IZ_b	IZ_c	IZ_d	IZ_k
0.04	5	140	0.02	0.2	-65	8	300

192 Further, to analyze the IZ model behavior across different spiking and bursting
193 behaviors, we have explored the parametric space (Table 2, Fig 3G) of
194 IZ_a, IZ_b, IZ_c, IZ_d & IZ_k (parameters in Eq. 4-5) within the boundaries identified in

Izhikevich, 2003 [31]. We investigated the IZ neuron model responses (Fig 3G) across 405 different parameter settings for each given input spike frequency. The parameter space was defined by the possible combinations of parameters listed in Table 2.

Table 2. Izhikevich neuron model parametric space explored in the evaluation of this study (for the IZ model presented in Fig 3G).

IZ_a	0.02	0.07	0.1	-	-
IZ_b	0.2	0.225	0.25	-	-
IZ_c	-65	-55	-50	-	-
IZ_d	2	4	8	-	-
IZ_k	100	200	300	400	500

Network connectivity

Our network was a two-layer fully connected neuronal network that comprised both inhibitory neurons (IN) and excitatory neurons (EN) (Fig 4A). The network architecture is defined based on the following two rules: (a) The sensory inputs are projected as excitatory synapses to all neurons in layer 1 only; (b) All excitatory and inhibitory neurons were fully reciprocally connected both within and between layers. Most of the analysis reported here utilized a "5×4" network architecture (5 ENs and 5 INs in layer 1 and 4 ENs and 4 INs in layer 2). In the analysis of Fig 8, where different network sizes were explored, we simply scaled up the number of neurons in each layer using the same connectivity rules (Fig 8).

A two-layer, fully reciprocally connected neuronal network architecture with self-recurrent connections (autapses) was also investigated. In this specific network architecture, in addition to the network connectivity defined above, the excitatory neurons projected excitatory synaptic

connections onto themselves, and inhibitory neurons projected inhibitory synaptic connections onto themselves (S7A Fig).

Sensory inputs

In this article, we investigated the individual neuron responses (Figs 2, 3 and S1-4 Figs) and network dynamics (Figs 4-8 and S6-7 Figs, except Fig 7C, D) based on six sensory inputs. These sensory inputs were pseudo-randomly generated (see below) and provided as excitatory input to both excitatory and inhibitory neurons. We also tested our recurrent networks with higher input sensor density (#sensors = 6, 15, 30 and 50, Fig 7C, D), the inputs of which were also pseudo-randomly generated.

Pseudo-random inputs: For the sensory inputs to the LSM and the IZ neurons, we generated pseudorandom spike trains for several different average frequencies (50, 100, 150 & 200 Hz, Fig 3A and S4 Fig) with uniform normal distributions. We used an inbuilt MATLAB® function "*randi"* to generate the spike time distributions in these spike trains. Furthermore, these spikes were convoluted to resemble post-synaptic-potentials (time continuous activity) using the following kernel equation [33],

$$a_i = \frac{\tau_{km}}{\tau_{kd} - \tau_{kr}} * \left[exp\left(\frac{-t - \tau_{kl} - t^*}{\tau_{kd}}\right) - exp\left(\frac{-t - \tau_{kl} - t^*}{\tau_{kr}}\right)\right] \quad (6)$$

Where, t^* is the input spike time, τ_{kd} is the decay time (4 ms), τ_{kr} is the rise time (12.5 ms) and τ_{km} is the constant to calculate ration between rise time and decay time (21.3 ms), and τ_{kl} is the latency time which is zero in this case. These values were chosen based on the previous work [12]. The convoluted sensor signal was then provided as synaptic input to the neuronal network.

In order to analyze the network dynamics, we provided 50 presentations of the same pseudorandom spike trains (for each given average frequency). Each input presentation

differed by an addition of random noise of ± 10 ms to individual spike times (Fig 3C, D, E, black lines) to the reference pseudorandom spike train (Fig 3A, for spike frequency of 50 Hz). These presentations were concatenated without pause or reset between them, so the input subdivided into 50 presentations was in effect one long presentation lasting for 50,000 ms.

To allow a comparison with the output of the LSM, we convoluted the output spike trains also of the spiking neuron model (IZ). The process of convolution emulated a post synaptic response that would have been generated in a receiving neuron, whereas the LSM output itself directly corresponded to such a signal.

Synaptic weights

All excitatory and inhibitory synaptic weights in the network were randomly distributed, including the excitatory sensory inputs to only the layer 1 neurons. The synaptic weight distributions were either normal, lognormal or binary. The normal and the log-normal distributions were generated for different mean weights (μ) (values between $0.1 - 0.5$) each with a fixed coefficiency of variation (cv) of 20% (where sigma $(\sigma) = (cv\ /\ 100) * \mu$). For binary distributions, we tested different probabilities of high weight synapses ($w = 1$) (probability varied between 10% - 50%), whereas the remainder of the synapses were set to zero weight (Fig 5A, B, C).

Statistical analysis

255 **Cross-correlation:** The correlation index measure was used to compute the similarity of the
256 responses of the neuron models (Fig 3F, G and S4E Fig). The correlation between two signals
257 was computed with an inbuilt MATLAB® function "*xcorr*" (with zero lag), which produces
258 values from 0 (uncorrelated) to 1 (identical).

259 **Frequency analysis:** We performed a continuous wavelet transform (using an inbuilt
260 MATLAB® function *'cwt'*) in order to define the frequency composition of the input signal
261 over time. The wavelet transform was used to extract the power of each frequency band as a
262 function of time for the continuous neuron activity signal. Here, we reported (Figs 4 – 8 and
263 S5-7 Figs), for each frequency band, the maximum power of the signal within each input
264 presentation time window (1 second).

265 In S5 Fig, the frequency analysis was performed on the sensory input signals (on the
266 convoluted signal for each given average spiking frequency) across all the 6 sensory inputs for
267 all 50 presentations (see Methods). The maximum power was computed for each sensory input
268 and each presentation, and the average across all 6 input sensors was reported in this figure.

269 In Fig 4, the frequency analysis was performed on the activity of one excitatory and
270 one inhibitory neuron in layer 1 (Fig 4B, C, F and G) across all frequencies and presentations.
271 S6 Fig display the frequency analysis performed on the activity of all excitatory and inhibitory
272 neurons in the network of Fig 4A. A similar frequency analysis was carried out in Figs 5-8 and
273 S5 Fig, which show the average maximum power calculated across all neurons in all layers and
274 across all 50 presentations.
275

276 # Results

277 ## Comparison to Spiking Neuron Models

278 We first characterized the input-output relationship of the neuron model in isolation
279 (Fig 3) for a standardized sensor input, consisting of randomized spike times in six sensor
280 neurons that were convoluted to time-continuous input signals. These were synaptically
281 integrated by a single modeled neuron (Fig 3A, B). The activity of the non-spiking LSM (linear
282 summation neuron model) was compared with that of a spiking neuron model (Izhikevich, IZ),
283 in terms of how well their output (Fig 3C-E) correlated with the input (Fig 3F). The IZ neuron
284 model was chosen for this comparison, as it was created to mimic a rich neuronal response
285 dynamics with computational efficiency [31]. The spikes generated by the IZ neuron model
286 were convoluted (see Methods) to a time continuous signal (Fig 3E) in order for it to be
287 comparable with the output of the LSM.

288 Both neuron models (LSM & IZ) were provided with the same pseudo-random sensory
289 inputs (average firing frequency of 50 Hz in each of six sensors, see Methods) connected via
290 six different synapses (Fig 3B). The IZ neuron model parameters for this particular comparison
291 (Fig 3E, F) were chosen to mimic the regular spiking behavior (hypothesized to be a common
292 neuron behavior in cortex [31,32]). The LSM neuron without dynamic leak reproduced on
293 average a close representation of the source convolution signal for the input but the individual
294 traces were considerably noisier without dynamic leak (Fig 3C) than with dynamic leak (Fig
295 3D). The main difference between the LSM and the IZ neuron model responses was that the IZ
296 neuron model tended to create output dynamic behavior that was not present in the input signal
297 (Fig 3B, E), a consequence of the binary nature of the spike output. A cross-correlation analysis
298 between the neurons' responses (Fig 3F) showed that the IZ neuron model reflected the input
299 signal less faithfully than the LSM. Note that the cross-correlation is slightly poorer for the

300 LSM with dynamic leak than without, which is due to that the some of the fine-timing details
301 of the high frequency components of the underlying convoluted signal is slightly filtered by
302 the dynamic leak.

303 We tested if this observation depended on the frequency of the spiking in the sensory
304 inputs. The LSM consistently showed a higher correlation with the input signal than the IZ
305 neuron model across a range of input spike frequencies (S3 Fig). Next we tested if the specific
306 parameters chosen for the IZ neuron model (Fig 3E, also indicated by an asterisk in Fig 3G)
307 were responsible for these results (Fig 3F). Therefore, we tested a range of parameter settings
308 (405 different parameter combinations), which are known to reproduce specific output
309 dynamics (bursting, for example) observed in a variety of neuron types *in vitro* [31]. The
310 correlation analysis showed that LSM was more consistent than the IZ model in maintaining
311 high correlation with the sensory inputs across the full range of sensory input spike frequencies
312 (Fig 3G). The exception was the highest sensory input frequencies, but that can be explained
313 by that the dynamics of the sensory input diminishes due to the density of the inputs (S3A-D
314 Fig), as previously described also for neurons *in vivo* [34]. This effect, which we will refer to
315 as the input density problem, is also evident in Fig 3G.

316 **Network dynamics (with and without Neuronal Dynamic Leak)**

317 We next investigated the activity dynamics of a standardized recurrent neuronal
318 network implemented using the LSM (Fig 4A). The sensory input was fed as excitatory input
319 to both the excitatory and inhibitory neurons of the first layer for 50 presentations, where the
320 sequential presentation differed by added Gaussian noise to the sensory signal (see Methods).
321 In the network with the neuron model without dynamic leak, there was initially a gradual
322 increase in the power across the higher frequency components of the activity in both excitatory
323 and inhibitory neurons (Fig 4B, C) (more extensively illustrated in S6 Fig, where the first few
324 presentations of sensory input evoked a lower power response). These high frequency

325 components were not present in the sensory input (S5A Fig) and were therefore generated by
326 the network, most likely as a consequence of the parallel excitatory and inhibitory connections,
327 which would be expected to lead to some degree of signal derivation [20]. Interestingly, in the
328 illustrated IN1 the high frequency components gradually built up (until presentation #10,
329 approximately) and then faded away (after presentation #20, approximately), despite that the
330 average intensity of the sensory input did not vary over time, which suggests a relatively rich
331 internal dynamics in this type of recurrent network, despite its limited size. In neurons of the
332 second layer, high frequency components typically faded away more slowly (S6 Fig). The
333 appearance of these high frequency components was sometimes associated with the appearance
334 of transients in the neuron activity (Fig 4D, E). In contrast, in the same network but with the
335 neuron model including the dynamic leak, the transients and the high-frequency components
336 of the neuron activity disappeared (Fig 4F -I). Hence, the low-pass filtering effect of the
337 dynamic leak 'rescued' the recurrent network from generating spurious high-frequency
338 components.

339 The recurrent connections of the network were likely strongly contributing to these
340 high-frequency components. An extreme case of recurrent connectivity is when a neuron makes
341 synapse on itself (autapse). It is not clear to what extent autapses exist in adult neuronal
342 circuitry, but they have been shown to be present in early development [35,36] and they are
343 widely used in the field of RNN/computational neuroscience [37]. To explore the impact of
344 autapses we used the exact same network architecture used in Fig 4 but added autapses to all
345 neurons (S7A Fig). In this scenario, the high-frequency components were strongly amplified
346 (S7B-E Fig). However, in the same network with the neuron model with the dynamic leak, the
347 transients and the high-frequency components of the neuron activity were again effectively
348 removed (S7F-I Fig). We did not explore networks with autapses any further.

349 We next compared the frequency power distributions of the neuronal activity in this
350 recurrent network across a range of different synaptic weight distributions (Fig 5). We studied
351 three different types of synaptic weight distributions (Gaussian, log-normal and binary
352 distributions). For each type of distribution, we tested five different mean synaptic weights (Fig
353 5A-C). Moreover, for each given synaptic weight distribution and mean weight, we generated
354 5 random weight distributions. The average signal of these 5 random weight distributions was
355 used to calculate each frequency power distribution illustrated (Fig 5D, E), where each line
356 represents the average activity across all the neurons of the network (Fig 5D, E). In the network
357 with the neuron model without dynamic leak (Fig 5D), the relative power of the high-frequency
358 components was amplified for synaptic weight distributions at mean synaptic weights of 0.3-
359 0.4 or above ($\mu \geq 0.4$ for Gaussian and $\mu \geq 0.3$ for log-normal distributions) and for $p > 10\%$
360 for binary distribution, compared to the sensory input (S5 Fig). For other synaptic weight
361 distributions ($\mu = 0.1$ for Gaussian and log-normal distributions and for $p = 10\%$ for binary
362 distributions, for example), there was much lower overall activity in the network, which could
363 be the reason why the high frequency components were not induced in these networks. In the
364 network with the neuron model with the dynamic leak component, the transients and the high-
365 frequency components of the neuron activity disappeared for all settings (Fig 5E), though the
366 setting of the dynamic leak component used also appeared to over-dampen the sensory input
367 dynamics between 20-200 Hz.

368 To further explore if the high-frequency components observed were induced by the
369 recurrent network, we tested if we could affect the 'center of gravity' of the high-frequency
370 components by introducing different conduction delays in signal transmission between the
371 neurons (Fig 6). In the brain *in vivo*, these would correspond to the axonal conduction delays
372 and synaptic delays combined. The delays were randomized between all the neurons, and
373 several different mean delays were tested in different simulations. Interestingly, the peak

374 frequency of the high-frequency component observed without dynamic leak (Fig 6A) was
375 approximately inversely proportional to the mean conduction delay. These peaks were removed
376 by adding dynamic leak (Fig 6B).

377 The high frequency components also appeared for lower average sensor input spike
378 frequency (50 & 100 Hz, Fig 7A) and for lower number of sensory inputs per neuron (nSensors
379 = 6 & 15, Fig 7C). In contrast, for higher input spike frequencies (150 & 200 Hz) and higher
380 number of sensory inputs (nSensors = 30 & 50) the increased density of the inputs resulted in
381 a paradoxical decrease in the power of the neuron activity across all frequencies analyzed (i.e.
382 as shown in S1 Fig), most likely due to the large number of randomized inputs regressing
383 toward the constant mean frequency of each sensory signal. In each case, in the network with
384 the neuron model with the dynamic leak component, the high-frequency components of the
385 neuron activity disappeared for the sensor input configurations where it had been present (Fig
386 7B, D).

387 We also explored if the size of the network could be a factor for the appearance of the
388 high frequency components. We found that these high frequency components appeared for
389 different network sizes and that in those cases the network activity was 'rescued' when the
390 LSM was implemented with the dynamic leak (Fig 8). Depending on the specific synaptic
391 weight distribution, the high frequency components became unequally dominant for different
392 network sizes (Fig 8A, E) according to unclear relationships. The largest network as a rule had
393 the weakest overall dynamics, which could be due to the same input density problem discussed
394 above, where the density of synaptic input increased as the larger network has a higher number
395 of recurrent synaptic inputs per neuron, which caused the dynamics of the neuron activity to
396 go down. As there is a tendency for membrane time constants to grow with the size of the
397 neuron [30], we scaled the τ_{Dyn} with the network size (as the neurons of the larger networks
398 had a higher number of synapses) (Fig 8C-D, and Fig 8G-H, for two different weight

distributions). A moderate scaling of the τ_{Dyn} (with the square root of the number of synapses, Fig 8C, G) actually increased the dynamics of some network sizes, while eliminating high frequency components. In contrast, a linear scaling (Fig 8D, H) instead appeared to dampen such dynamics and, unsurprisingly, low pass-filtered also signals well below 100 Hz for the largest networks.

Discussion

In the present paper, we explored the properties of a non-spiking neuronal model, which was derived from the differential conductance-based H-H model, in various recurrent neuronal networks. We found that in these recurrent networks, many different factors would tend to trigger network induction of high frequency signal components of a somewhat unpredictable magnitude and distribution (i.e. Figs 5-8). These signal components were not present in the input data (S5 Fig) and sometimes peaked to create overt spurious transients (Fig 4B, C). The dynamic leak in our neuron model invariably 'rescued' the recurrent networks from their tendency to self-generate these high-frequency signal components (Figs 4-8; S7 Fig). Corresponding to the capacitive component and the ion channels of the membrane circuit, dynamic leak is an inevitable feature of real neurons. Furthermore, this low-pass filter component made the behavior of recurrent networks more predictable for networks of different sizes.

We worked under the scenario that neuronal networks in the brain are recurrent and that excitatory and inhibitory connections are both pervasive, without any a priori assumed structure. Our network architecture contained the circuitry elements of previously reported 'classical' network connectivity patterns (feedback and feedforward inhibition, for example). Feed-forward and feedback inhibition running in parallel with excitatory connections was likely the main network feature that caused the signal derivation effects/the high frequency components in the networks without the dynamic leak. The inclusion of autapses in the recurrent network strongly amplified these high frequency components (S7 Fig), presumably primarily through self-amplification of excitatory neurons. But note that in a recurrent network, any local circuity feature will at the global level automatically result in other functional network features as well. Hence, in contrast to a non-recurrent, feed forward neuronal network, in a recurrent network these circuitry features will hence become less clear-cut from a

430 functional point of view, which could cause additional dynamic network effects that for
431 example could explain our observations of gradual build-up of high frequency power
432 components (Fig 4 and S5 Fig) while there was steady sensory input level to keep the network
433 activity up. However, understanding such network dynamics at a deeper level was outside the
434 scope of this paper, but would need to be addressed if such networks are to be used in a
435 functional setting.

436 In our recurrent networks, apparently spurious high frequency components could be
437 induced for different types of synaptic weight distributions, delays between neurons, sensory
438 input densities and network sizes. It was hard to predict under what exact conditions such high
439 frequency components would become more or less dominant (i.e. Fig 8), but in each case the
440 dynamic leak effectively cancelled them out. From the point of view of the functionality of a
441 processing recurrent network, the fact that the frequency distribution of any given network did
442 not match that of the sensory input is not automatically to be considered a disadvantage because
443 the goal of a processing network would not be to perfectly replicate the sensory input. However,
444 the fact that these high frequency components sometimes took the shape of clear-cut transients
445 with no obvious counterpart in the sensor signal suggests that, at least in part, they should be
446 considered spurious, i.e. noise injected into the signal due to the dynamics of the specific
447 network.

448 In some cases, the activity of the network became highly suppressed relative to the
449 sensory input (i.e. for low mean weights in Fig 5 and for the largest network in Fig 8). This
450 effect can be ascribed to the input density problem, i.e. when too many unrelated but
451 continuously active synaptic inputs converge on the same neuron, their signal dynamics would
452 tend to cancel out, leaving the neuron with very little signal dynamics [34]. As these signals,
453 due to the network structure, are paralleled by inhibitory connections, when the signal

454 dynamics is lost, inhibition and excitation cancel each other out and the activity dynamics is
455 lost in the network as a whole.

456 How would spiking neuron networks fare with respect to rescuing a recurrent network
457 from spurious high frequency components? The phasic nature of discrete spike output would
458 be expected to worsen the problem, whereas refractoriness would tend to dampen it.
459 Refractoriness could certainly rescue the system from the extreme transients observed in
460 networks that included autapses. Refractoriness, however, would not rescue the system from
461 high frequency components generated through longer range recurrent excitatory loops.

462 Recurrent neuronal networks with balanced excitatory and inhibitory synaptic
463 connections have been extensively studied previously [22,23,38,39], using spiking neuron
464 models (employing integrate-and-fire or related mechanisms for the spike generation). In these
465 studies, the recurrent connections were sparsely distributed with an overall connection
466 probability of 1-2%, and a ratio of 4:1 excitatory to inhibitory interneurons. These studies point
467 out that factors such as high connection probability and unbalanced excitation-inhibition tend
468 to produce network instability [39] and in some cases failure in signal propagation across the
469 layers of those neuronal networks [22]. From the stability we observed across a wide range of
470 recurrent network configurations, always at 100% connection probability (though weighted),
471 it would seem that the LSM with dynamic leak would be beneficial for ensuring stable recurrent
472 neuronal network behavior across a range of network sizes and density of connectivity.

473 The present findings suggest that the biological feature of neuronal dynamic leak, which causes
474 the polarization (i.e. the activity) of the neuron to settle towards resting potential with a time
475 constant, is an important functional feature. It allows brain networks to fully utilize recurrent
476 neuronal network architectures with variable numbers of participating neurons without risking
477 self-generated noise embodied as high frequency components and spurious transients.
478

Acknowledgments: Funding: This work was supported by the EU Grant FET 829186 ph-coding (Predictive Haptic COding Devices In Next Generation interfaces), the Swedish Research Council (project grant no. K2014-63X-14780-12-3).

References

1. Binzegger T, Douglas RJ, Martin KAC. A quantitative map of the circuit of cat primary visual cortex. J Neurosci. 2004. doi:10.1523/JNEUROSCI.1400-04.2004

2. Kar K, DiCarlo JJ. Fast recurrent processing via ventral prefrontal cortex is needed by the primate ventral stream for robust core visual object recognition. bioRxiv. 2020. doi:10.1101/2020.05.10.086959

3. Koestinger G, Martin KAC, Rusch ES. Translaminar circuits formed by the pyramidal cells in the superficial layers of cat visual cortex. Brain Struct Funct. 2018. doi:10.1007/s00429-017-1588-7

4. Song S, Sjöström PJ, Reigl M, Nelson S, Chklovskii DB. Highly nonrandom features of synaptic connectivity in local cortical circuits. PLoS Biology. 2005. doi:10.1371/journal.pbio.0030068

5. Hooks BM, Mao T, Gutnisky DA, Yamawaki N, Svoboda K, Shepherd GMG. Organization of cortical and thalamic input to pyramidal neurons in mouse motor cortex. J Neurosci. 2013. doi:10.1523/JNEUROSCI.4338-12.2013

6. Steriade M. Synchronized activities of coupled oscillators in the cerebral cortex and thalamus at different levels of vigilance. Cereb Cortex. 1997. doi:10.1093/cercor/7.6.583

7. Allen GI, Tsukahara N. Cerebrocerebellar communication systems. Physiological Reviews. 1974. doi:10.1152/physrev.1974.54.4.957

8. Jörntell H. Cerebellar physiology: links between microcircuitry properties and sensorimotor functions. Journal of Physiology. 2017. doi:10.1113/JP272769

9. Obermayer J, Heistek TS, Kerkhofs A, Goriounova NA, Kroon T, Baayen JC, et al. Lateral inhibition by Martinotti interneurons is facilitated by cholinergic inputs in human and mouse neocortex. Nat Commun. 2018. doi:10.1038/s41467-018-06628-w

10. Douglas RJ, Martin KAC. Inhibition in cortical circuits. Current Biology. 2009. doi:10.1016/j.cub.2009.03.003

11. Zhu JJ, Lo FS. Recurrent inhibitory circuitry in the deep layers of the rabbit superior colliculus. J Physiol. 2000. doi:10.1111/j.1469-7793.2000.00731.x

12. Rongala UB, Spanne A, Mazzoni A, Bengtsson F, Oddo CM, Jörntell H. Intracellular dynamics in cuneate nucleus neurons support self-stabilizing learning of generalizable tactile representations. Front Cell Neurosci. 2018. doi:10.3389/fncel.2018.00210

13. Swadlow HA. Fast-spike interneurons and feedforward inhibition in awake sensory neocortex. Cerebral Cortex. 2003. doi:10.1093/cercor/13.1.25

14. Isaacson JS, Scanziani M. How inhibition shapes cortical activity. Neuron. 2011. doi:10.1016/j.neuron.2011.09.027

15. Jörntell H, Ekerot CF. Receptive Field Plasticity Profoundly Alters the Cutaneous Parallel Fiber Synaptic Input to Cerebellar Interneurons In Vivo. J Neurosci. 2003. doi:10.1523/jneurosci.23-29-09620.2003

16. Pi HJ, Hangya B, Kvitsiani D, Sanders JI, Huang ZJ, Kepecs A. Cortical interneurons that specialize in disinhibitory control. Nature. 2013. doi:10.1038/nature12676

17. Sultan KT, Shi SH. Generation of diverse cortical inhibitory interneurons. Wiley Interdisciplinary Reviews: Developmental Biology. 2018. doi:10.1002/wdev.306

18. Okun M, Lampl I. Instantaneous correlation of excitation and inhibition during ongoing and sensory-evoked activities. Nat Neurosci. 2008. doi:10.1038/nn.2105

19. Anderson JS, Carandini M, Ferster D. Orientation tuning of input conductance, excitation, and inhibition in cat primary visual cortex. J Neurophysiol. 2000. doi:10.1152/jn.2000.84.2.909

20. Wehr M, Zador AM. Balanced inhibition underlies tuning and sharpens spike timing in auditory cortex. Nature. 2003. doi:10.1038/nature02116

21. Sutskever I, Vinyals O, Le Q V. Sequence to sequence learning with neural networks. Advances in Neural Information Processing Systems. 2014.

22. Vogels TP, Abbott LF. Signal propagation and logic gating in networks of integrate-and-fire neurons. J Neurosci. 2005. doi:10.1523/JNEUROSCI.3508-05.2005

23. Brunel N. Dynamics of sparsely connected networks of excitatory and inhibitory spiking neurons. J Comput Neurosci. 2000. doi:10.1023/A:1008925309027

24. Liou JY, Smith EH, Bateman LM, Bruce SL, McKhann GM, Goodman RR, et al. A model for focal seizure onset, propagation, evolution, and progression. Elife. 2020. doi:10.7554/eLife.50927

25. Chakravarthy N, Tsakalis K, Sabesan S, Iasemidis L. Homeostasis of brain dynamics in epilepsy: A feedback control systems perspective of Seizures. Ann Biomed Eng. 2009. doi:10.1007/s10439-008-9625-6

26. Naundorf B, Wolf F, Volgushev M. Unique features of action potential initiation in cortical neurons. Nature. 2006. doi:10.1038/nature04610

27. Spanne A, Geborek P, Bengtsson F, Jörntell H. Spike generation estimated from stationary spike trains in a variety of neurons In vivo. Front Cell Neurosci. 2014. doi:10.3389/fncel.2014.00199

28. Saarinen A, Linne ML, Yli-Harja O. Stochastic differential equation model for

553 cerebellar granule cell excitability. PLoS Comput Biol. 2008.
554 doi:10.1371/journal.pcbi.1000004

555 29. Spanne A, Jörntell H. Questioning the role of sparse coding in the brain. Trends in
556 Neurosciences. 2015. doi:10.1016/j.tins.2015.05.005

557 30. Zhang ZW. Maturation of Layer V Pyramidal Neurons in the Rat Prefrontal Cortex:
558 Intrinsic Properties and Synaptic Function. J Neurophysiol. 2004.
559 doi:10.1152/jn.00855.2003

560 31. Izhikevich EM. Simple model of spiking neurons. IEEE Trans Neural Networks.
561 2003;14: 1569–1572. doi:10.1109/TNN.2003.820440

562 32. Izhikevich EM. Which model to use for cortical spiking neurons? IEEE Trans Neural
563 Networks. 2004;15: 1063–1070. doi:10.1109/TNN.2004.832719

564 33. Mazzoni A, Panzeri S, Logothetis NK, Brunel N. Encoding of naturalistic stimuli by
565 local field potential spectra in networks of excitatory and inhibitory neurons. PLoS
566 Comput Biol. 2008;4. doi:10.1371/journal.pcbi.1000239

567 34. Bengtsson F, Ekerot CF, Jörntell H. In vivo analysis of inhibitory synaptic inputs and
568 rebounds in deep cerebellar nuclear neurons. PLoS One. 2011.
569 doi:10.1371/journal.pone.0018822

570 35. Lübke J, Markram H, Frotscher M, Sakmann B. Frequency and dendritic distribution
571 of autapses established by layer 5 pyramidal neurons in the developing rat neocortex:
572 Comparison with synaptic innervation of adjacent neurons of the same class. J
573 Neurosci. 1996. doi:10.1523/jneurosci.16-10-03209.1996

574 36. Tamás G, Buhl EH, Somogyi P. Massive autaptic self-innervation of GABAergic
575 neurons in cat visual cortex. J Neurosci. 1997. doi:10.1523/jneurosci.17-16-
576 06352.1997

37. Graves A. Supervised Sequence Labelling. 2012. doi:10.1007/978-3-642-24797-2_2

38. Vogels TP, Sprekeler H, Zenke F, Clopath C, Gerstner W. Inhibitory plasticity balances excitation and inhibition in sensory pathways and memory networks. Science (80-). 2011. doi:10.1126/science.1211095

39. Rubin R, Abbott LF, Sompolinsky H. Balanced excitation and inhibition are required for high-capacity, noise-robust neuronal selectivity. Proc Natl Acad Sci U S A. 2017. doi:10.1073/pnas.1705841114

40. Hodgkin a L, Huxley a F. A quantitative description of membrane current and its applicaiton to conduction and excitation in nerve. J Physiol. 1952. pp. 500–544. doi:10.1016/S0092-8240(05)80004-7

41. Tougaard J. Signal detection theory, detectability and stochastic resonance effects. Biol Cybern. 2002. doi:10.1007/s00422-002-0327-0

42. Lindner B. Low-pass filtering of information in the leaky integrate-and-fire neuron driven by white noise. Understanding Complex Systems. 2014. doi:10.1007/978-3-319-02925-2_22

APPENDIX 1

Neuron model derivation from H-H model

We first describe the rationale for our Linear Summation neuron model (LSM). In brief, the LSM aims to provide a simple and computationally efficient neuron model, while capturing important characteristics of H-H conductance models [12,40]. The membrane potential in the LSM model is normalized between +1 and -1 with a resting potential of zero. The output of an LSM neuron is a continuous, non-spiking signal that reflects the portion of the membrane potential that exceeds some threshold, which we assumed to be the zero resting potential. This would be suitable to represent one neuron or a population of similarly connected neurons that is biased by background activity to be at or near spontaneous activity (such as is hypothesized for stochastic resonance to prevent dead bands)[41]. This continuous output signal is intended to reflect the mean spike rate that a population of similarly connected neurons would transmit to other centers in the nervous system.

In H-H models the various ion channels associated with ionic pumps and leaks define a resting membrane potential where there are no net currents. Any change in membrane potential away from this resting potential will settle back to the resting potential according to the combined conductance of all of these ion channels, which is called the static leak. Synaptic activation leads to opening of specific ion channels, which in the H-H models as a change of synaptic conductance. The ion(s) that are made permeable by the synapse have a reversal potential that is different from the resting membrane potential. When the ion channels of a particular synapse are open, the membrane potential will be driven towards that reversal potential, with a strength that depends on the strength of the synaptic conductance relative to the static leak conductance.

The synaptic currents charge the neuron, which is modeled as a single capacitor (assuming that the electrotonic distances between different parts of the neuron are negligible). Various synaptic signals are thus integrated and converted into a dynamically changing membrane potential. The static leak is in parallel with this capacitor, thereby defining a time-constant τ for these dynamic changes. The effect is that of low-pass filtering of the integrated synaptic currents [42] to produce the membrane potential that defines the output state of the neuron. In an H-H model, the output state is created by converting the membrane voltage into patterns of spike output, with the help of a threshold for spike generation. Spike generation is omitted in the LSM model and the output of the neuron is instead the part of the membrane potential that exceeds some threshold (herein equal to the resting membrane potential).

First, we describe a conductance-based model similar to previously presented models [12,40] and then show how a model similar to the LSM model can be derived. In this category of ion channel conductance-based models, the dynamics of one type of ion channel is lumped together into one single conductance. Compared to other conductance-based models, no spike generation is modeled and the neurons resting potential is set to zero. The neuron is modeled as a capacitor with capacitance (C) and is charged by excitatory ($I_{syn,exc}$) and inhibitory synaptic currents ($I_{syn,inh}$) and discharged by a leak current (I_{leak}). Therefore, the neurons membrane potential (V) measured across the capacitor follows the following equation.

$$C\frac{dV}{dt} = I_{leak} + I_{syn,exc} + I_{syn,inh} \tag{A1}$$

The leak current is set proportional to the membrane potential by constant conductance g_L according to Ohm's law:

$$I_{leak} = -g_L V \tag{A2}$$

If the synaptic currents are zero, the neuron's membrane potential will decay to zero. Therefore, this model neuron's resting membrane potential is zero. At each excitatory synapse i the firing rate of the presynaptic neuron (v_i^+) produces a current. The synapse has a baseline conductance (w_i^+), called synaptic weight. This conductance is scaled by the presynaptic neuron's firing rate. The direction and magnitude of the current is determined by the difference between the constant reversal potential (E_{exc}) and the neuron's membrane potential. For an excitatory synapse, the current would reverse if the membrane potential rose above the positive reversal voltage, so synaptic activity can never produce a membrane potential about the reversal potential. Therefore if the neuron has already reached this voltage, the neuron's voltage cannot increase further. The current contributed by an individual synapse can be modeled as

$$I_{syn,exc_i} = -(V - E_{exc})w_i^+ v_i^+ \tag{A3}$$

The same model is applied for the current generated by an inhibitory synapse i, with reversal potential (E_{inh}), synaptic weight (w_i^-) and presynaptic firing rate (v_i^-). The reversal potential of an inhibitory synapse is set so that the neurons potential cannot decrease below this potential.

$$I_{syn,inh_i} = -(V - E_{inh})w_i^- v_i^- \tag{A4}$$

Summing all synaptic currents and plugging in the current equations into the membrane potential equation we obtain

$$C\frac{dV}{dt} = -g_L V - \sum_i (V - E_{exc})w_i^+ v_i^+ + \sum_i (V - E_{inh})w_i^- v_i^- \tag{A5}$$

where the first sum is over all excitatory synapses and the second sum over all inhibitory synapses. In order, to show the relationship of this equation to the LSM model, we set the leak conductance to one and replace leak conductance and membrane capacitance by a time constant τ. The reversal potentials are set to +1 and -1 for the excitatory and the inhibitory synapses,

respectively. Hence the range of possible membrane potential is between +1 and -1, assuming that the initial voltage is also in that range.

The resulting differential equation is

$$\tau \frac{dV}{dt} = -V + (1 - V) \sum w_j^+ v_j^+ + (1 + V) \sum w_k^- v_k^- \tag{A6}$$

This equation can be solved by applying the implicit Euler method. Let V_t be the membrane voltage in timestep t and h the stepsize. The following equation must be solved for V_{t+1}

$$V_{t+1} = V_t + h \frac{1}{\tau} \left(-V_{t+1} + (1 - V_{t+1}) \sum w_j^+ v_j^+ + (1 + V_{t+1}) \sum w_k^- v_k^- \right) \tag{A7}$$

In this case an analytic solution is possible:

$$V_{t+1} = \frac{V_t + \frac{h}{\tau} \sum w_i v_i}{1 + \frac{h}{\tau} + \frac{h}{\tau} \sum |w_i| v_i} \tag{A8}$$

where both sums are over all synapses.

The parameters of this model are also listed in S1 Table. This new system has components not commonly found in neuron models. The reason is that usually the differential equation describes an instantaneous effect of the inputs and the state of the neuron. In this system the effect of the input on how the input is processed by the neuron in a future time step is already considered.

From the above derivation (Eq. A8) we could observe that the excitatory ($I_{syn,exc}$) and inhibitory ($I_{syn,inh}$) synaptic currents from a conductance based neuron model (Eq. A1), can be reduced to a total synaptic weight summation $\left(\frac{\sum wV}{1+\sum |w| V}\right)$, and that the leak current (I_{leak}) (Eq. A1), which is a dynamic leak because it occurs across capacitor, can be reduced to h/τ (a dynamic leak constant, Eq. A8; if this constant is larger than zero and smaller than one, it can

be disregarded in this expression). Based on this neuron model derivation, we propose the simplified linear summation neuron model (LSM, A10) to capture the essential dynamics of the original H-H conductance-based model (S1 Fig). The LSM is given by two equations: LSM without dynamic leak (Eq. A9) and LSM with dynamic leak (Eq. A10).

$$A_{No_{Dyn}} = \frac{\sum(w_i a_i)}{1 + \sum|w_i a_i|} \tag{A9}$$

$$\frac{\tau_{Dyn} * dA_{Dyn}}{dt} = -A_{Dyn}(t) + A_{No_{Dyn}}(t) \tag{A10}$$

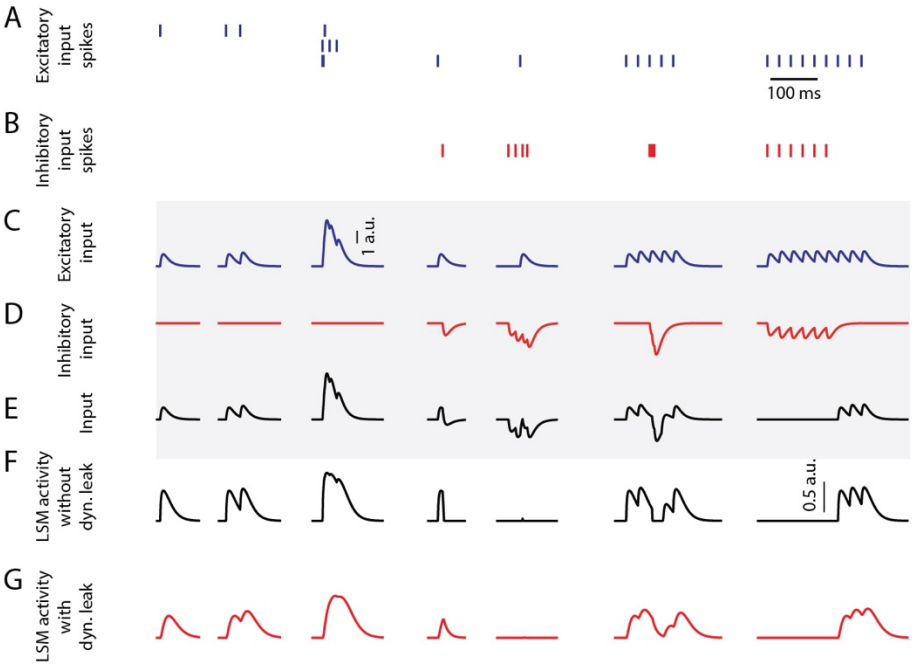

Fig 1. LSM responses to emulated synaptic inputs. (**A**) The activation times of three different excitatory synaptic inputs are indicated as spike trains. (**B**) The activation times of one inhibitory synaptic input. (**C-D**) The excitatory and inhibitory sensory input spike trains were convoluted using a kernel function (see Methods) to create input that resembles post-synaptic potentials. Note that the input to the LSM neuron can exceed 1 a.u., while the output of the LSM neuron cannot. Calibration applies to C –E (traces in the shaded region). (**E**) The input from summation of the excitatory and inhibitory inputs. (**F**) LSM (without dynamic leak, $k_{static} = 1$) output activity for the given PSP inputs. Calibration applies to F-G. (**G**) LSM (with dynamic leak, $k_{static} = 1, \tau_{dyn} = 1/100\,\mathrm{s}$) output activity for the given PSP inputs.

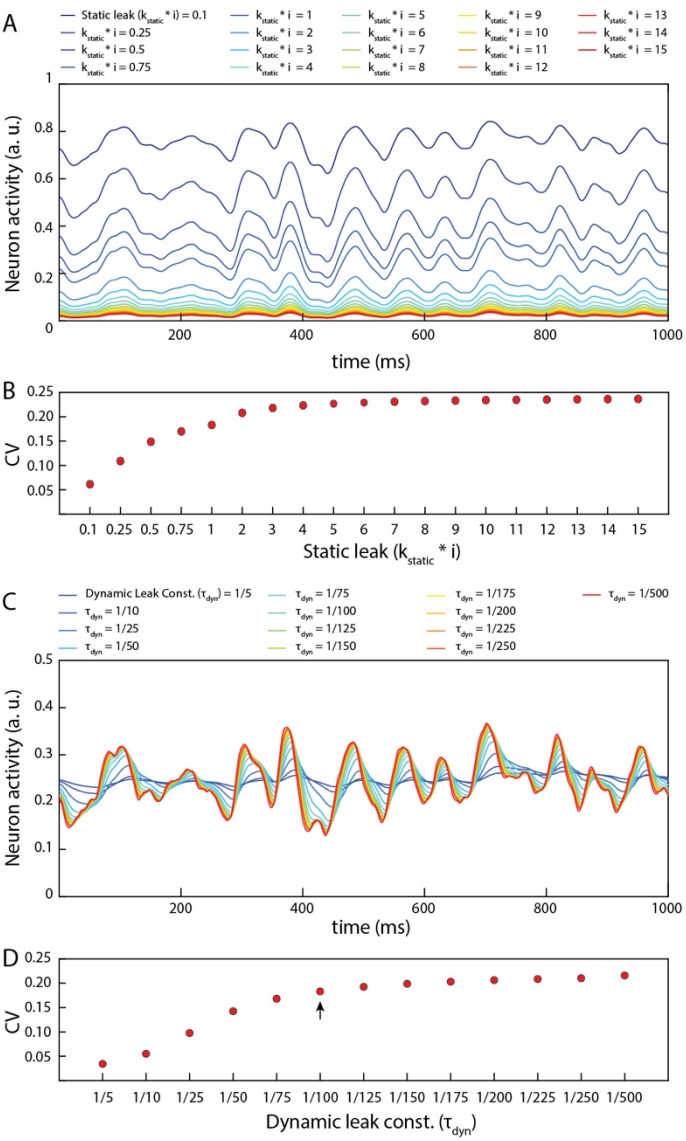

Fig 2. Impact of static leak (k_{static}) and dynamic leak constant (τ_{dyn}) in LSM. (**A**) Impact of the value of k_{static} in the LSM (for $\tau_{dyn} = 1/100$) for a given pseudo-random sensory input at 50 Hz for each of six sensors (see Fig 3). (**B**) The perseverance of dynamics in the neuron activity (A) for varying k_{static} value as assessed by the coefficient of variation ($CV = \sigma(A)/\acute{A}$) . A higher value of CV indicates a higher activity variance relative to the mean activity. (**C**) Impact of the value of τ_{dyn} in the LSM (for $k_{static} = 1$) for the same pseudo-random sensory input as in **A**. (**D**) The CV as a function of the value of the dynamic leak (τ_{dyn}) in the LSM. The arrow indicates the value of τ_{dyn} used in rest of this paper unless otherwise specified.

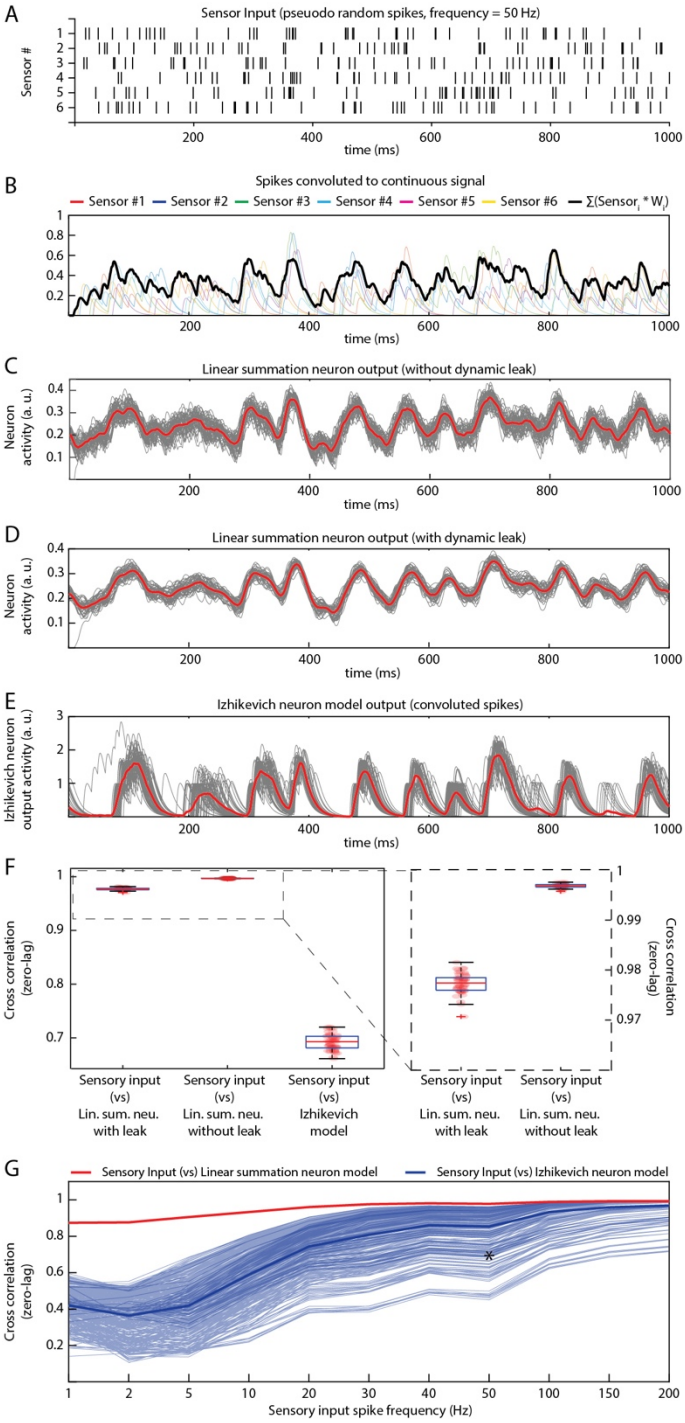

Fig 3. Comparing the properties of different neuron models in isolation. (A) Pseudo-random input spike trains (six spike trains corresponding to the six sensory inputs, with an average spike frequency of 50 Hz in each sensor) **(B)** The sensory input spike trains were convoluted using a kernel function (see Methods). The convoluted input responses were fed as weighted (randomly generated, mu = 0.4) EPSP inputs to the neuron model. (**C**) Output responses of the LSM without dynamic leak. The red line is the mean across 50 presentations

(each presentation made different by adding Gaussian noise, black lines). In this and all panels below, tests were made for the neuron in isolation, without network connections. (**D**) Similar display as in **C**, but for LSM with dynamic leak. (**E**) Similar display as in **C**, but for output responses of Izhikevich neuron model. The spike output of the Izhikevich neuron model were convoluted using a kernel function (same kernel parameters setting as in **B**). (**F**) Cross-correlations between the sensory input and the output responses of neuron models (illustrated in **C-E**). (**G**) Cross-correlation between different sensory input frequencies and neuron model outputs across a range of IZ model settings, compared to the LSM with dynamic leak. Thin blue lines indicate the cross-correlation with the sensory input for the IZ neuron model responses for each of the 405 IZ model parameter settings ($\mathrm{IZ_a}, \mathrm{IZ_b}, \mathrm{IZ_c}, \mathrm{IZ_d}$ and $\mathrm{IZ_k}$ see methods) tested. Thick blue line indicates the mean of those cross-correlations. The red line indicates the cross-correlation between the sensory inputs and the LSM outputs. Asterisk indicates the cross-correlation measure for the parameters chosen in Fig 3F.

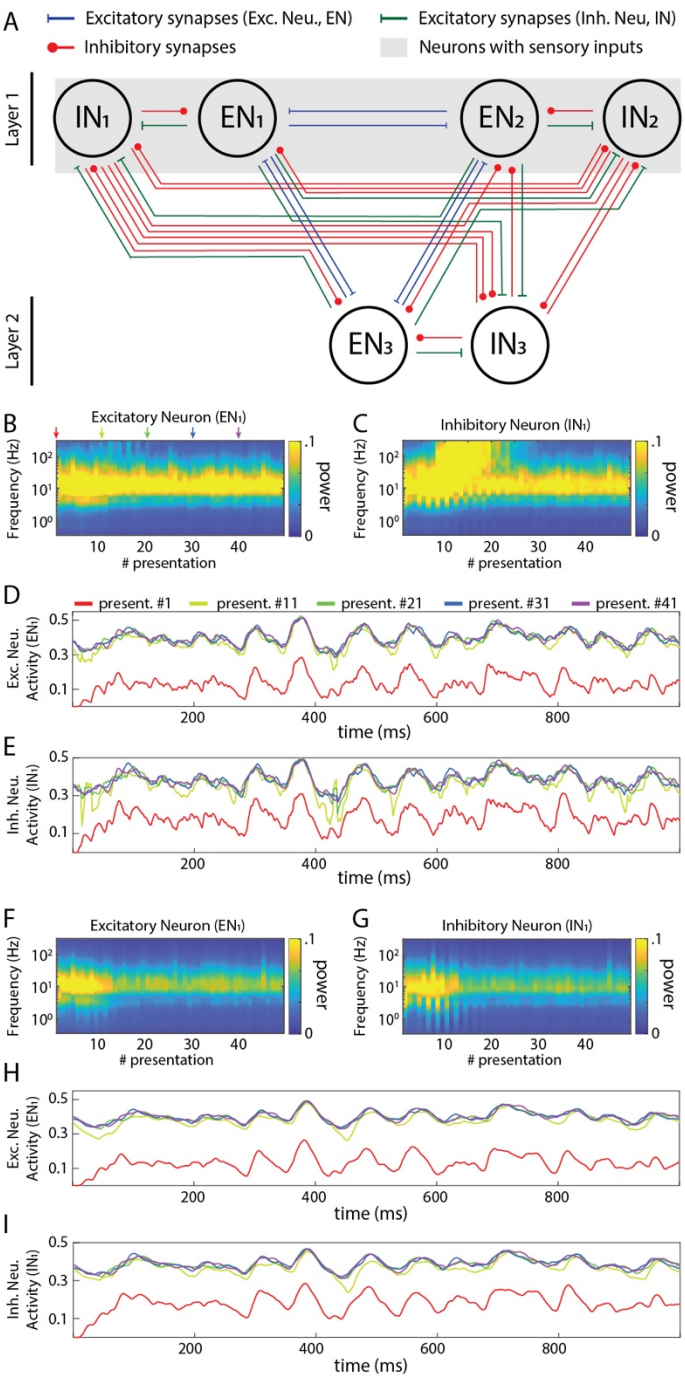

Fig 4. Activity dynamics in a sample recurrent network. (**A**) Principles of the connectivity structure in the recurrent network studied. Note that the default network, and the one used in panels **B-I** of this figure, contained excitatory neurons (5 in the input layer, 4 in the output layer) and inhibitory neurons (same numbers) with the same connectivity whereas only the neurons in layer 1 also received sensory inputs (the same 6 sensory inputs to each neuron) with all synapses having randomly generated gaussian weights (mu = 0.4). (**B**) Frequency plot of

the activity in an excitatory neuron. (**C**) Similar plot for an inhibitory neuron. (**D**) Raw data plots for sample signals in the excitatory neuron generated at the indicated presentation #. (**E**) Similar plot for the inhibitory neuron. (**F**)-(**I**) Similar plots as in (**B**)-(**E**) but when all the neurons were modelled to include the neuronal dynamic leak.

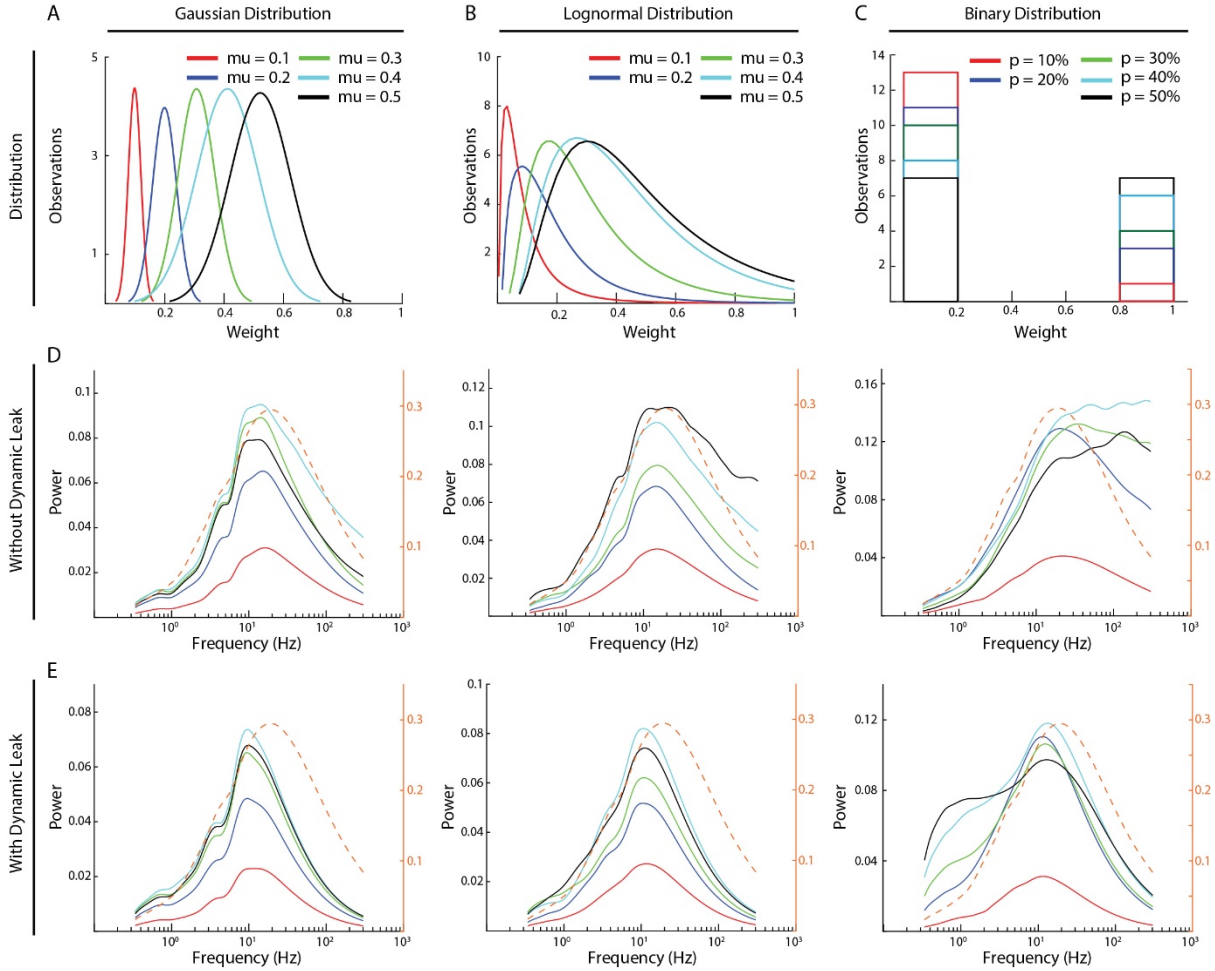

Fig 5. High frequency components and the effect of dynamic leak across different synaptic weight distributions. (**A-C**) The three types of synaptic weight distributions that were explored (Gaussian, Log-Normal and Binary) and the average weight distributions for each mean weight value (five weight distributions were generated for each mean weight). (**D**) The frequency power distributions across all the above synaptic weight distributions. Color keys for the different average synaptic weights are in A-C. (**E**) Similar display as in C, for the same networks but with the neuron model with dynamic leak. Dashed orange traces in D, E show the corresponding frequency power distribution for the sensory inputs at 50 Hz, averaged across the six sensory inputs, for comparison.

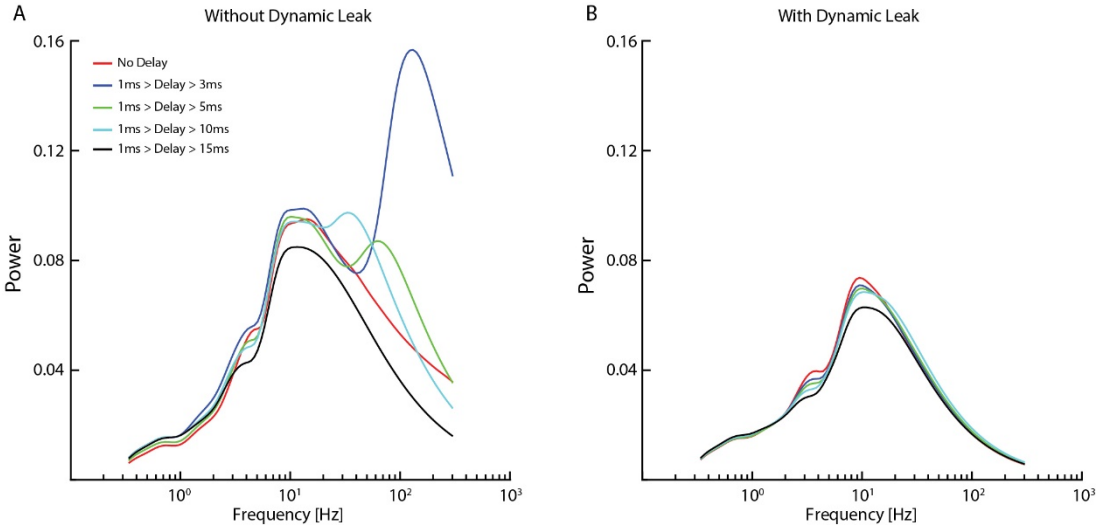

Fig 6. Impact of conduction delays on the frequency distribution. (**A**) Frequency distributions for the same network (network settings as in Fig 4) with different average conduction delays between neurons. (**B**) Data for the same networks and delays when the neuron model included dynamic leak.

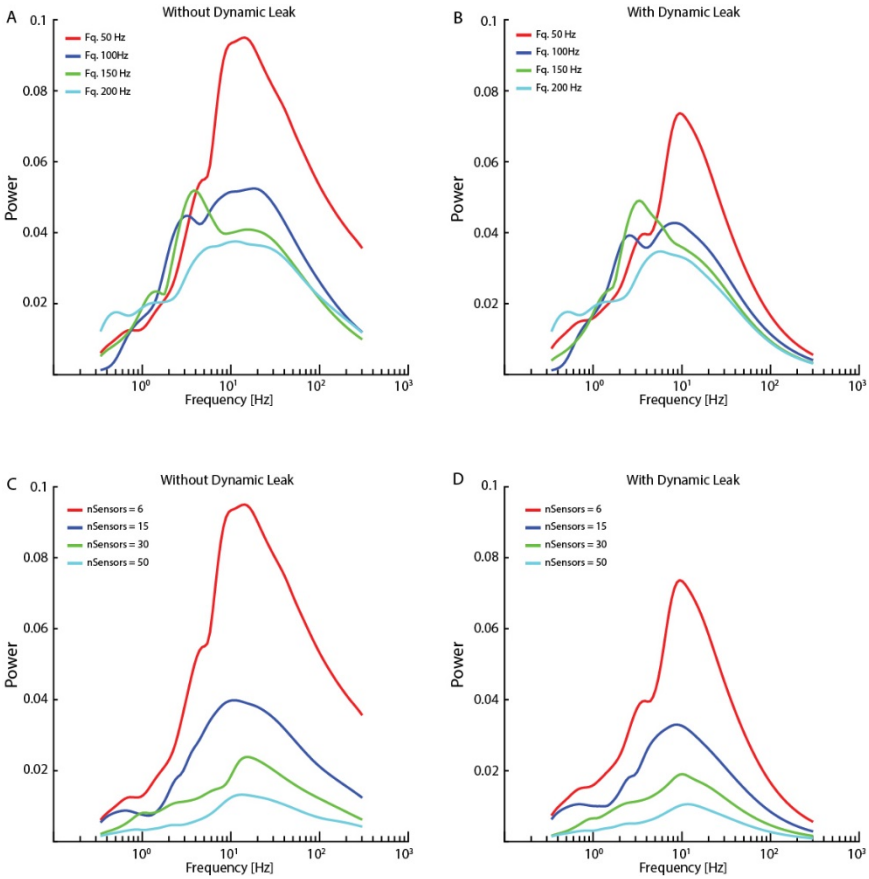

Fig 7. Network activity dynamics increased when sensor input density decreased. (**A**) The high frequency components became more prominent with lower average spike frequencies in the sensor input. (**B**) Neuronal dynamic leak resulted in disappearance of the high-frequency components across all input spike frequencies. (**C**) The high frequency components also became more prominent with lower number of sensory inputs, while a very high number of sensor inputs substantially reduced overall neuron activity dynamics. (**D**) Introduction of neuronal dynamic leak resulted in disappearance of the high-frequency components irrespective of the number of sensory inputs. The network settings for this analysis were similar to Fig 4, except for sensory input.

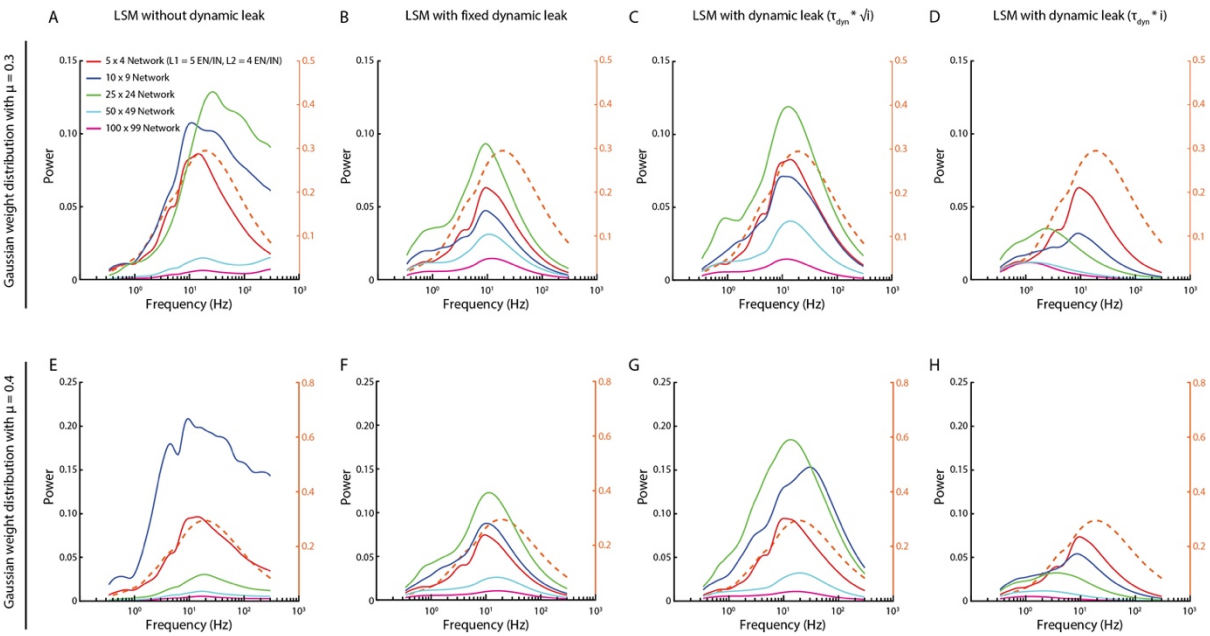

Fig 8. Activity frequency distributions altered with the scale of the networks. (**A, E**) For networks with Gaussian synaptic weight distribution of mean weight mu = 0.3 and 0.4, respectively, the high frequency components could appear without dynamic leak, regardless of network size. (**B, F**) Introduction of the neuronal dynamic leak ($\tau_{\mathrm{dyn}} = 1/100$) 'rescued' the networks from these high-frequency components. (**C, G**) The dynamic leak constant was adapted based on the square root of number of synapses (i)**.** (**D, H**) The dynamic leak constant was adapted based on the total number of synapses (i). Dashed orange traces in all plots show the corresponding frequency power distribution for the sensory inputs at 50 Hz, averaged across the six sensory inputs, for comparison.

Supporting Information

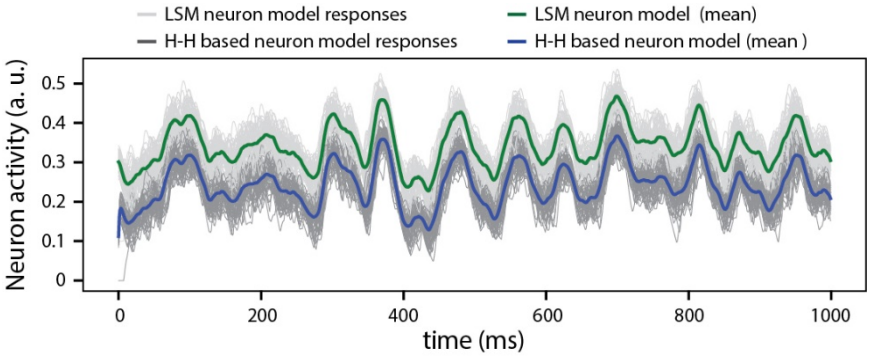

S1 Fig. Signal similarity between the LSM **and H-H model.** A comparison between the output responses for LSM (green line is the mean across 50 presentations) and the H-H (derived using backward Euler method, blue line is the mean across 50 presentations), for a given pseudo-random sensory input at 50 Hz for each of six sensors (see Fig 3). The responses of the LSM output were offset by 0.1 activity (a.u.) in order to visualize the coherence between the responses of both neuron models. The cross correlation (with zero lag) was 0.99.

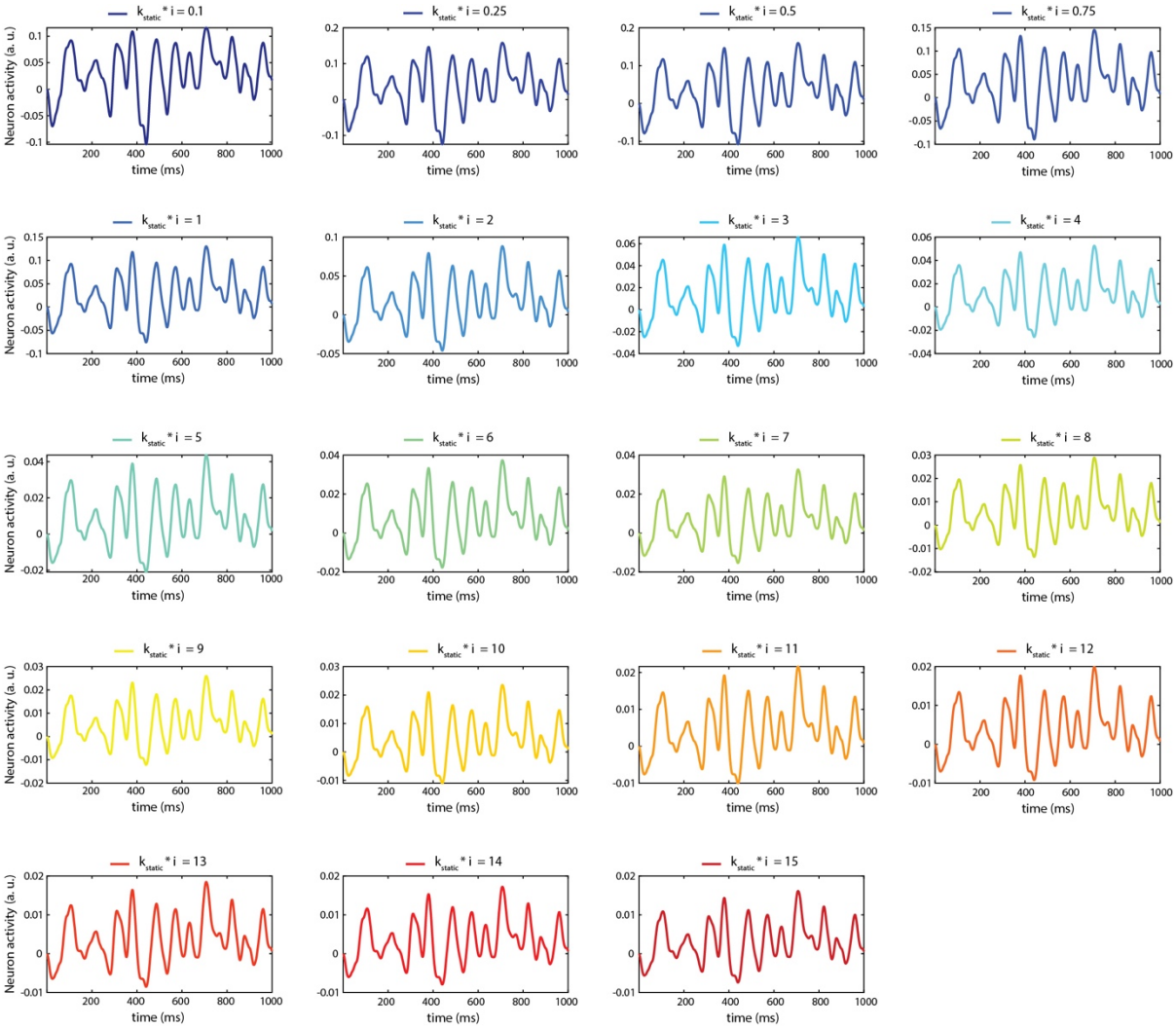

S2 Fig. Impact of the value of k_{static} on the internal activity of the LSM for a given sensory input.

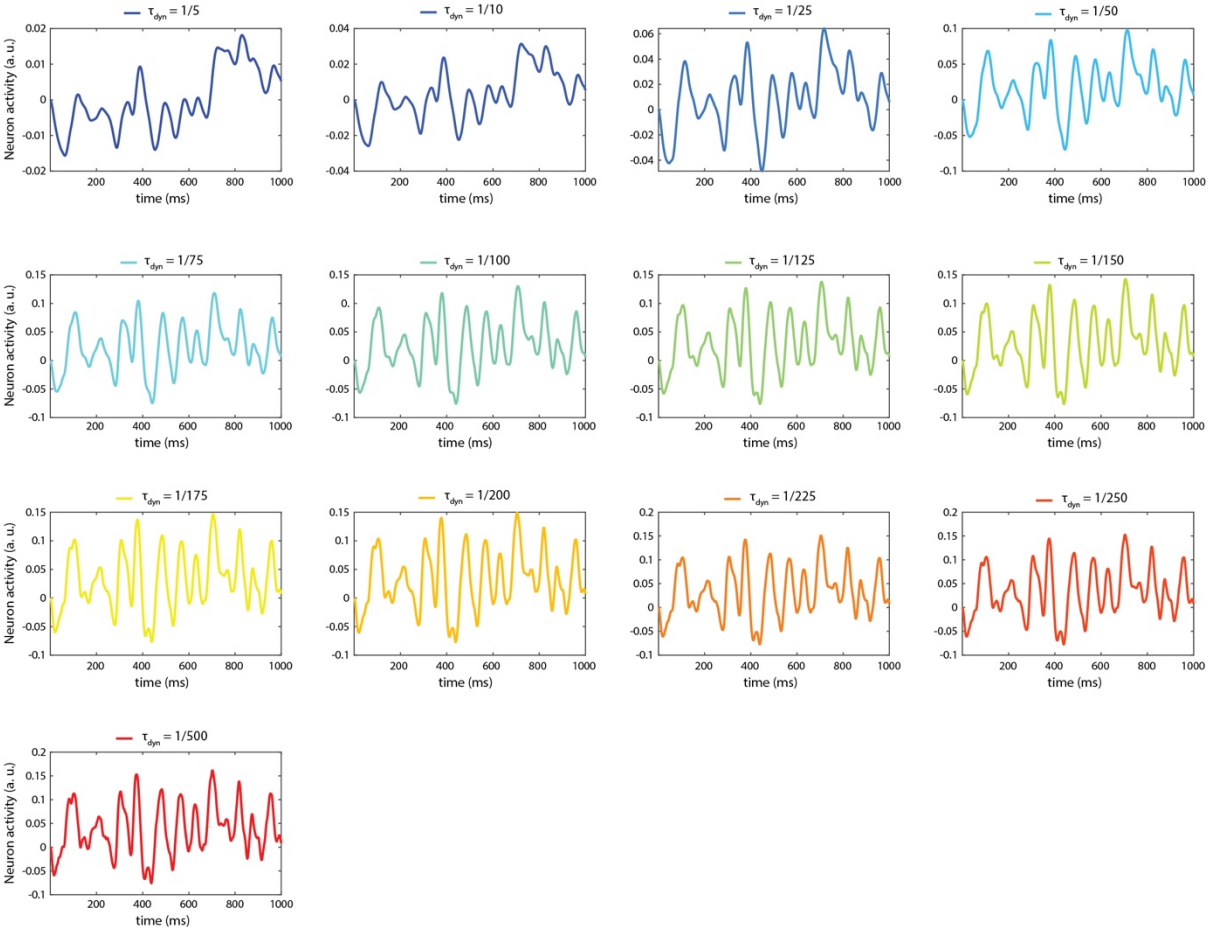

S3 Fig. Impact of the value of τ_{dyn} on the internal activity of the LSM for a given sensory input.

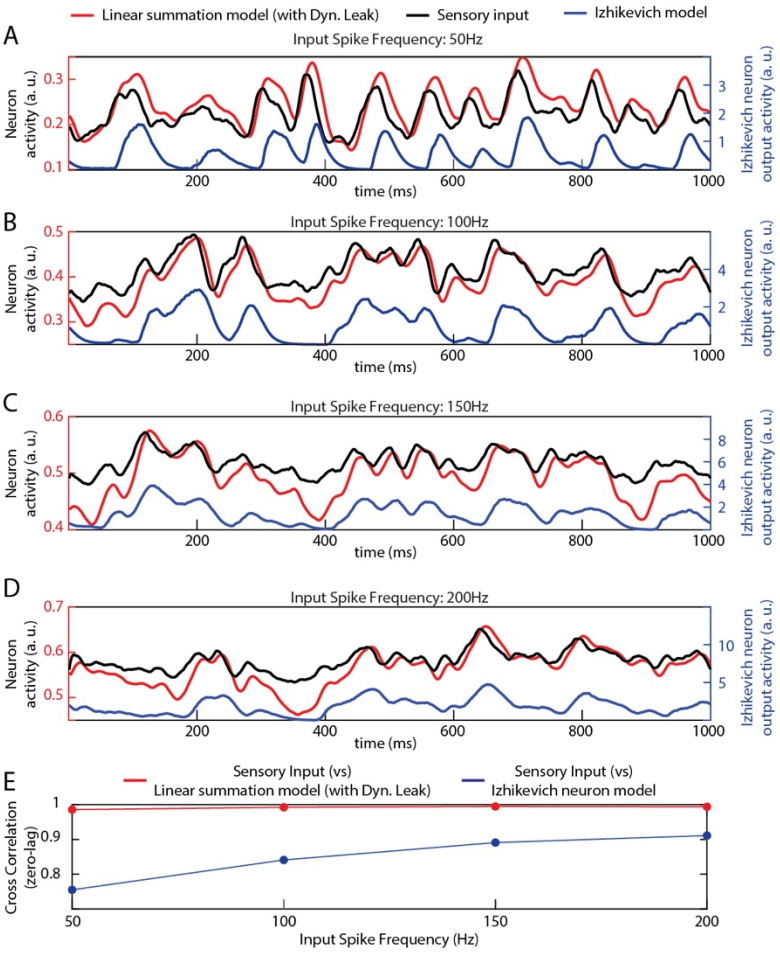

S4 Fig. Comparison of the non-spiking and the spiking neuron model outputs for different sensory input frequencies. (**A-D**) Neuron outputs in response to different sensory input frequencies. (**E**) Cross-correlation between sensory inputs and the neuron model outputs.

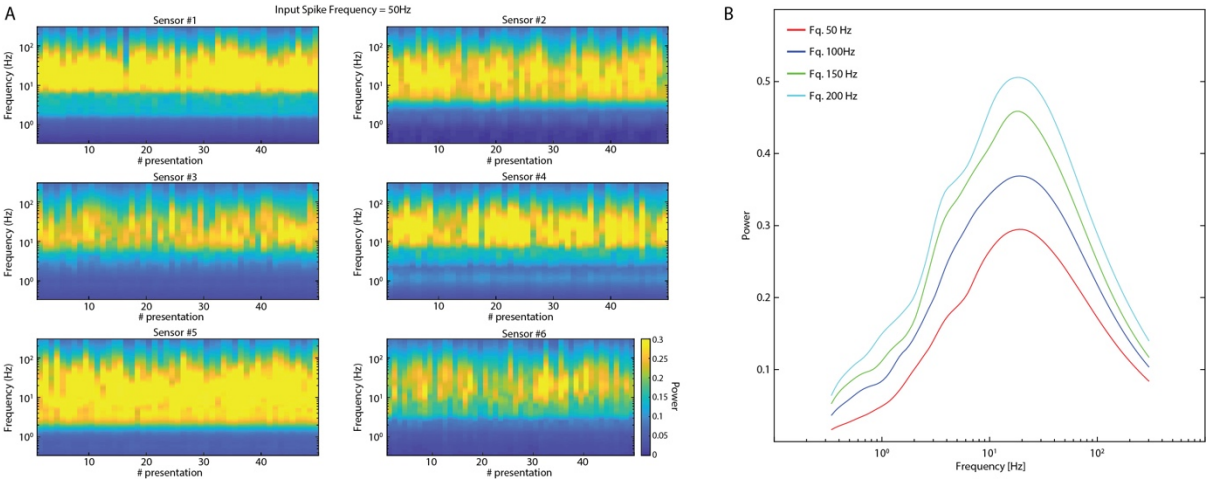

S5 Fig. Frequency analysis of the sensory inputs. (**A**) Time-continuous frequency power analysis for each of the six sensory inputs (spike frequency = 50Hz) across the 50 presentations used in the analysis of the network activity. (**B**) Frequency power analysis (using continuous wavelet transform, see Methods), of sensory inputs. The plots show the average power of the activity across all the six sensors, for each of the four mean sensor firing frequencies, across all 50 presentations used in the analysis of the network activity.

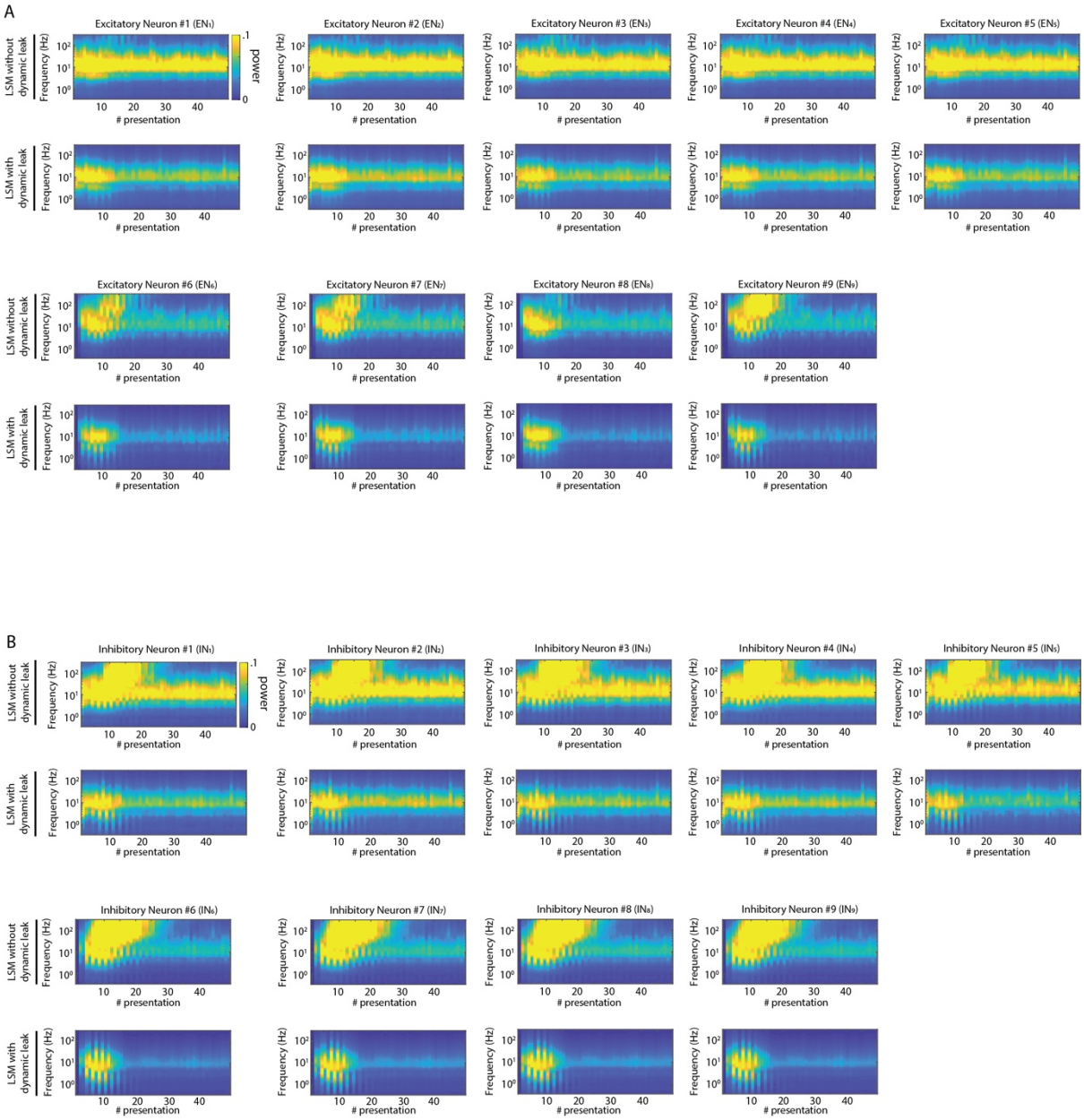

S6 Fig. Frequency analysis plots of the activity in all excitatory neurons ($EN_1 - EN_9$) and inhibitory neurons ($IN_1 - IN_9$) for the network shown in Fig 4A.

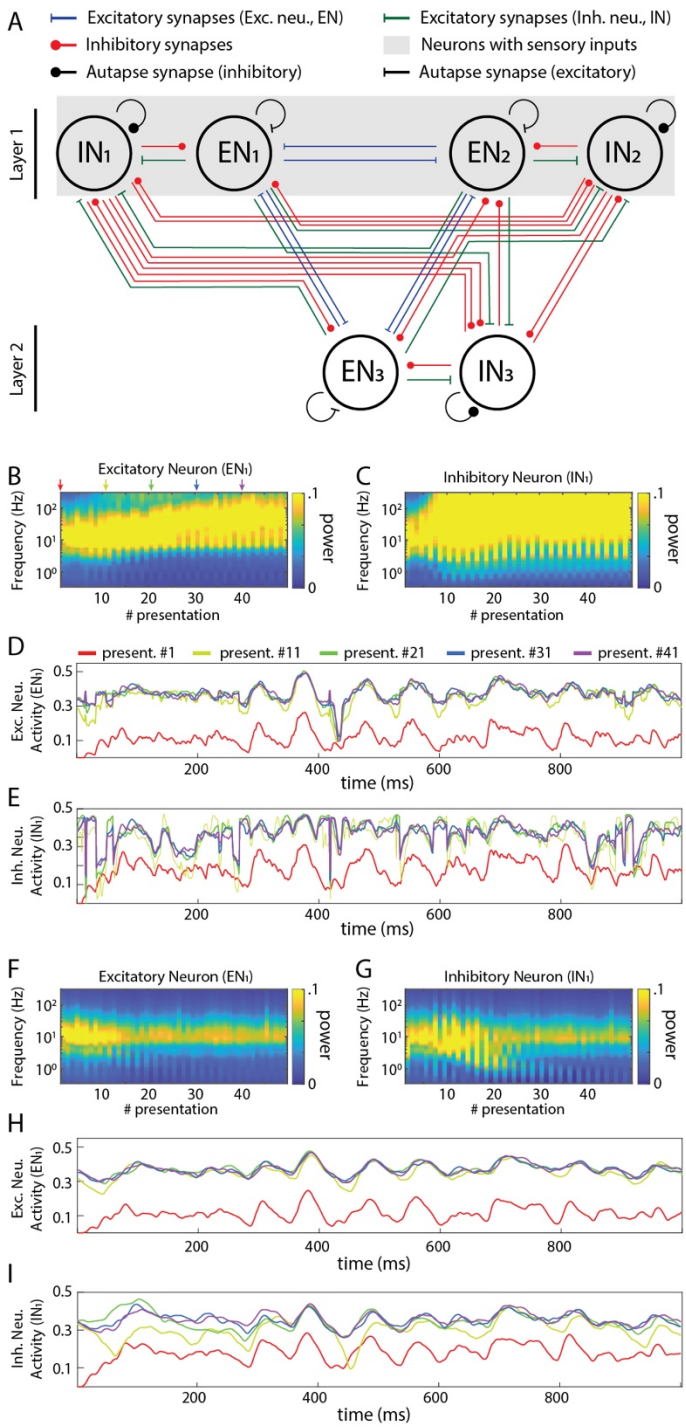

S7 Fig. Activity in recurrent networks with autapses. (**A**) Principles of the connectivity structure in the recurrent network studied. The network presented here is a fully connected network as in Fig 4, with the addition of self-recurrent excitatory and inhibitory synapses (in excitatory and inhibitory neurons, respectively). (**B**) Frequency plot of the activity in an excitatory neuron. (**C**) Similar plot for an inhibitory neuron. (**D**) Raw data plots for sample signals in the excitatory neuron generated at the indicated presentation #. (**E**) Similar plot for

the inhibitory neuron. (**F**)-(**I**) Similar plots as in (**B**)-(**E**) but when all the neurons were modelled with the dynamic leak.

Parameter	Symbol	Units
Membrane potential	V	[V]
Membrane capacitance	C	[F]
Membrane time constant	τ	[s]
Time step	h	[s]
Neuron output	v	[V]
Excitatory weights	w_i	[1]
Inhibitory weights	w_j	[1]
Presynaptic excitatory neuron activity	V_i^+	[V]
Presynaptic inhibitory neuron activity	V_j^-	[V]
Excitatory currents	I_{exc}	[A]
Inhibitory currents	I_{inh}	[A]
Leak currents	I_{leak}	[A]

S1 Table. H-H Model variable definitions (for the H-H neuron model derivation, presented in APPENDIX 1).